LEPS proposal for Q-PAC
Title : Backward-meson photoproduction up to 2.9 GeV

Spokesperson: Mizuki Sumihama RCNP Osaka University,
researcher, e-mail:sumihama@rcnp.osaka-u.ac.jp

September 18, 2009

Collaborator list

Name	affrication	position
M. Sumihama	Osaka Univ. (RCNP)	Researcher
T. Hotta	Osaka Univ. (RCNP)	Assistant professor
T. Nakano	Osaka Univ. (RCNP)	Professor
K. Ozawa	The Univ. of Tokyo	Lecturer
Y. Morino	Osaka Univ. (RCNP)	Researcher
M. Oka	Osaka Univ. (RCNP)	Administrative assistant
M. Niiyama	RIKEN	Researcher
N. Muramatsu	Osaka Univ. (RCNP)	Assistant Professor
Y. Kato	Osaka Univ. (RCNP)	Administrative assistant
T. Yorita	Osaka Univ. (RCNP)	Assistant professor
J. K. Ahn	Pusan National Univ.	Associate Professor
D. S. Ahn	Osaka Univ. (RCNP)	Administrative assistant

Beam running time: 90 days

Requirements for the beam condition and experimental equipment:

Linearly polarized photon beam with 1.5 GeV−2.9 GeV energies

Liquid hydrogen target (cylindrical shape, 15 cm thickness)

LEPS forward spectrometer

Lead-plastic sandwich detector

Contents

1 Summary of proposal

Recently, the LEPS collaborators measured differential cross sections for π^0, η, η', and ω photoproductions, and photon asymmetries for π^0 photoproduction at backward angles with photon energies from 1.5 GeV to 2.4 GeV. Several interesting behaviors have been observed for these reactions. However, none of them have been understood well. We believe these data shed light to the problem of missing baryon resonances around 2 GeV, and the u-channel nucleon exchange process.

In order to provide more information on these behaviors, we would like to propose an experiment of backward meson photoproductions extending the photon energy up to 2.9 GeV, and installing new detectors. In this experiment, we will obtain both differential cross sections and photon asymmetries for $\pi^0, \eta, \eta', \omega, \rho^0$, and ϕ photoproductions. The lead-plastic sandwich detector will be installed around the target to detect charged particles and γ rays from mesons. Background events will be reduced and the signal to noise ratio will be improved with this detector.

2 Physics motivation

2.1 Baryon resonances

Many resonances around 2 GeV predicted in the constituent quark model have not been identified experimentally [1]. Identification of these missing resonances is important to investigate whether the quark-model calculations are valid or not. Information on baryon resonances mainly comes from the pion induced productions. A part of missing resonances may not couple to a pion channel strongly but couple to other channels. So that it has been realized that pion induced reactions are limited to search for missing resonances. The photon beam is good mean to search for missing resonances because there are various channels in the final state. Recently, pion, kaon, η and η' photoproductions have been measured in many facilities [2, 3, 4, 5, 6, 7, 8]. The experimental data have been analyzed connecting with N* or Δ^* resonances [9, 10]. However no resonance has been newly proved yet. This is partly because some weakly excited resonances are obscured due to other strong resonances which have large decay widths, making it difficult to demonstrate their existence only from a specific channel or only from cross section data. Therefore, it could be useful to perform comprehensive studies with various channels in order to extract resonances. Alternatively, polarization observables are useful to extract missing resonances because interference between resonances could be seen.

2.2 u-channel process at backward angles

At very backward angles, the production mechanism is dominated by the u-channel process where a proton or a nucleon resonance is exchanged. In general, differential cross sections of meson photoproduction are well described using a simple equation of $s^{2\alpha(u)-2}$ on basis of the Regge theory at high energies [11, 12]. Unfortunately, the applicability of Regge theory is not well demonstrated at lower energies because of the lack of experimental data. The LEPS collaborators have obtained the s-dependence of differential cross sections, $d\sigma/du$, for ω photoproduction at the total energies, $W = 1.9 - 2.3$ GeV [13]. Figure 1 shows the results from LEPS and Daresbury [14]. The s-dependence from the LEPS data is different from that from the Daresbury data, which is well explained by nucleon Regge pole [14]. It is very interesting to measure ω photoproduction up to $W = 2.55$ GeV, and see how the LEPS data connect to the Daresbury data. The measurement of other meson photoproductions is also interesting to investigate the u-channel nucleon exchange process.

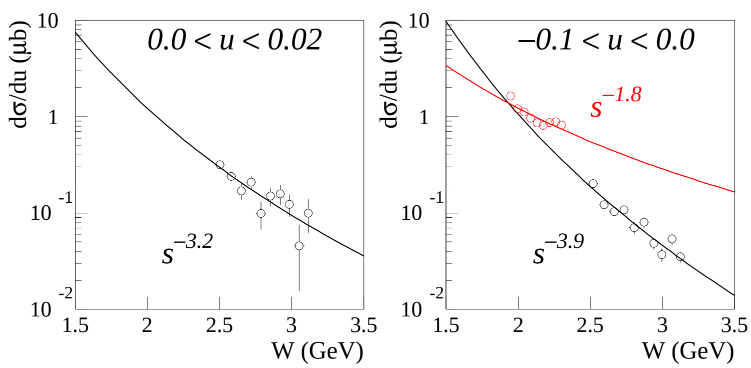

Figure 1: W ($\sqrt{s}$) dependence of differential cross sections, $d\sigma/du$, for ω photoproduction. open black circles and open red circles are the data from Daresbury [14] and LEPS, respectively. the solid curves are results of a fit to the data. the range of $0.0 < u$ is not valid kinetically in the LEPS energy region.

2.3 $s\bar{s}$ knockout process from proton

The unpolarized cross section and photon beam asymmetry for ϕ photoproduction at backward angles will help to understand a contribution from the $s\bar{s}$ direct knockout process from a proton [15]. A experiment of double polarization observables (beam-target) for ϕ photoproduction is planed, and the polarized target is now under construction at the LEPS facility [16]. The double polarization observables are very sensitive to the strangeness content of a proton because these observables can distinguish the knockout process with other processes [15]. The proper energy for the double polarization measurement will be known by obtaining the energy dependence of differential cross sections at backward angles.

2.4 Meson photoproductions in the previous experiment

Figure 2 shows the missing mass spectrum for the $\gamma p \rightarrow pX$ reaction obtained by detecting protons with the LEPS forward spectrometer in the previous experiment. Peaks due to π^0, η, η', ω and ϕ productions are identified. Background events from non-resonant multi-pion photoproductions exist under the signal peaks of single-meson photoproductions. The missing mass distributions for each photoproduction were generated in the Monte Carlo simulation by taking into account the detector resolution. The experimental data were fitted by using all the generated missing-mass distributions. The contribution of each reaction channel were determined by changing the relative height of the distribution in order to minimize the fitting χ^2. The experiment was carried out at $E_\gamma = 1.5 - 2.4$ GeV.

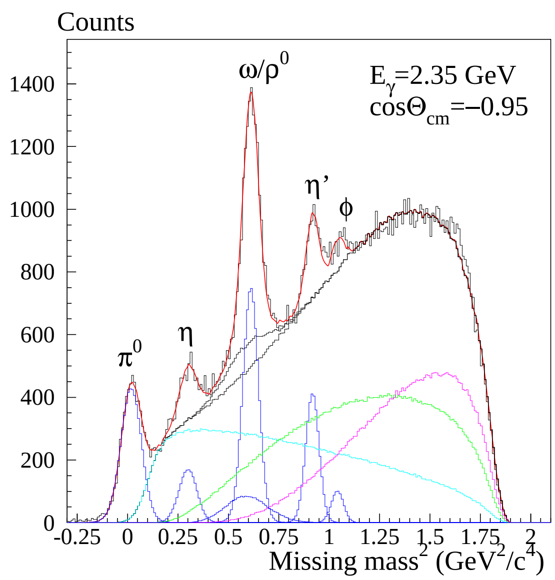

Figure 2: Spectrum of missing mass square for protons at $E_\gamma = 2.3 - 2.4$ GeV and $\cos\Theta_{c.m.} = -1.0 - -0.9$, where $\Theta_{c.m.}$ is a scattering angle of mesons in the center-of-mass system. Red curve shows the fitting. The light-blue, green and pink curves are for non-resonant 2π, 3π and 4π production, respectively. The black-dotted curve is the sum of these multi-pion reactions and ρ^0 production. The blue histograms are for single meson photoproductions.

Figure 3 and 4 show photon beam asymmetries and differential cross sections for π^0 photoproduction obtained in the previous LEPS experiment, respectively [8]. A strong angular

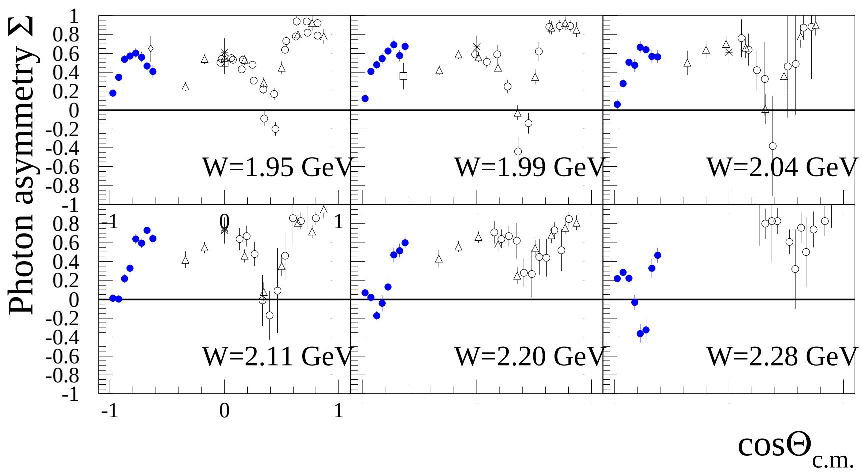

Figure 3: Photon beam asymmetries Σ as a function of the π^0 scattering angle, cos$\Theta_{c.m.}$. The closed circles are the results from LEPS. The range of photon energies, E_γ [GeV], is indicated in each plot. The other plots are the data from other facilities, ▫ [17], △ [18], ○[19], ∗ [20].

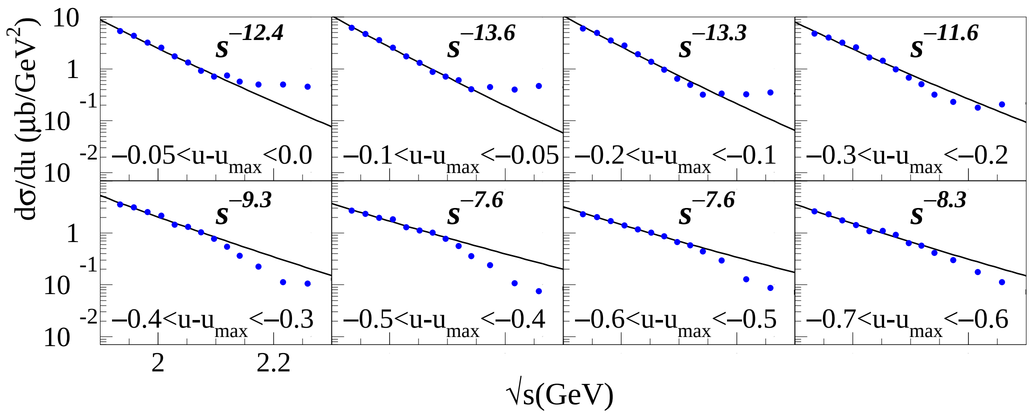

Figure 4: Differential cross sections as a function of the total energy, $\sqrt{s}$, for the $\gamma p \rightarrow \pi^0 p$ reaction. The range of $u - u_{\max}$ [GeV^2] is indicated in each plot. The closed circles are the results from LEPS. The curves are the fitting results of As^{-x} for the data at $\sqrt{s}$ <2.1 GeV, where A and x are fitting parameters [14].

dependence of the photon asymmetry appears above $W > 2.1$ GeV. There is a dip structure around $\cos\Theta_{c.m.} = -0.8$. The data drop to a negative sign, and then rise up to a positive sign in the narrow angular range. The differential cross sections sharply decrease with increasing energies up to 2.1 GeV. The slope is about -12 at $u - u_{\max} > -0.3$ while it is about -8 at $u - u_{\max} < -0.3$. Above 2.1 GeV, the cross sections do not follow with the fitting curves determined by the data at lower $\sqrt{s}$.

Figure 5 shows differential cross sections for η, η', ω and π^0 photoproductions. A wide bump structure is observed above 2.0 GeV in η photoproduction. A small bump structure is observed around 2.25 GeV in η' photoproduction. There is no prominent structure for the ω photoproduction cross-section. The cross section for π^0 photoproduction drastically decreases with energies up to 2.15 GeV and shows a mostly flat distribution above 2.15 GeV. The energy dependences of differential cross sections for π^0, η, η' and ω photoproductions differ. The comprehensive studies of these channels will help to improve theoretical calculations for determining the resonance states contributing to these channels, and understanding the mechanism of meson photoproductions. Figure 6 shows photon asymmetries measured in

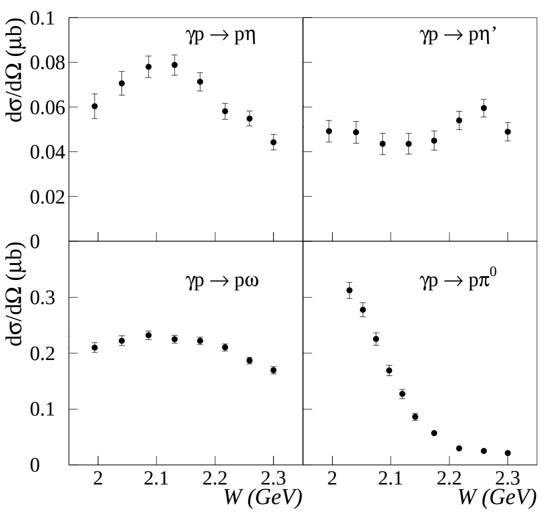

Figure 5: Differential cross sections for η, η', ω and π^0 photoproductions plotted as a function of the total energy (W) at $\cos\Theta_{c.m.} = -0.7 - -0.8$

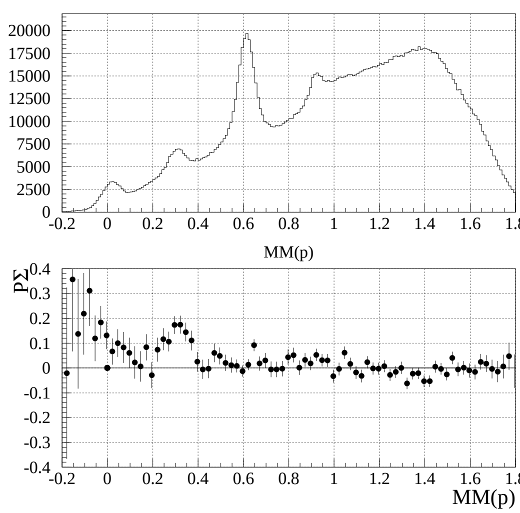

Figure 6: Top : Missing mass square of protons. Bottom : Photon asymmetries as a function of missing mass square.

the previous experiment. The peak structure was observed in the range of η meson peak of missing mass square. Photon asymmetries for η photoproduction seem to be a positive sign. In the other range of the missing mass square, there is no structure. The large contribution of background events may conceal photon asymmetries of single-meson photoproductions.

The differential cross sections and photon asymmetries for various meson photoproductions up to $E_\gamma = 2.9$ GeV will provide more information for the interesting behaviors observed in the previous experiment.

3 Experimental method

In this experiment, we will obtain both differential cross sections and photon asymmetries for π^0, η, η', ω, ρ^0 and ϕ photoproductions at $E_\gamma = 1.5 - 2.9$ GeV and at $\cos\Theta_{c.m.}$ $-1 - -0.6$ where $\Theta_{c.m.}$ is an angle of mesons in the center-of-mass system. The LEPS forward spectrometer will be used to detect protons at forward angles. Mesons will be identified with a missing mass technique. Background events from non-resonant multi-pion productions $(2\pi, 3\pi, 4\pi)$ will be reduced, and the ρ^0 and ω will be separated by using the lead-plastic sandwich detector surrounding the target.

3.1 Existing equipments

- The LEPS forward spectrometer and the tagging system will be used in this experiment. All devices will be used at the same position and the same conditions as the LEPS standard setup except for the start counter. The start counter will be replaced to a larger plastic scintillator. The dipole magnet will be excited with the normal value, 800 A.

- The target system for liquid hydrogen, which is used for the NTPC experiment, will be used (see Fig. 7). The cell is cylindrical. The length is 15 cm, and the diameter is 4 cm. The outer diameter of the chamber (nose) is 8 cm. The target will be positioned at z = –998 mm (the position of the center of magnet is z=0), where is the same as the position of the LEPS standard setup for the long LH2/LD2 target.

- The trigger condition will be the same as that of the standard setup. The trigger will be made by a coincidence signal of signals from the tagging system, the start counter, and TOF wall with a veto signal from the aerogel counter. We will not use any signal from the lead-plastic sandwich detector placed around the target. The trigger rate is expected to be about 30 Hz with the tagger rate of 500 kcps. The expected dead time is a few %.

- We will use the existing DAQ system. Additionally, 24 channels of ADC and TDC will be used for the lead-plastic sandwich detector.

3.2 Laser system

We will use a high power deep-UV laser, UV50 from SONY, to produce the linearly polarized photon beam. The wave length of laser is 266 nm ($E_\gamma^{max} = 2.89$ GeV). The power is 2W, which is about double power of the existing Ar laser. We expect 500 kcps for the beam intensity of tagged photons with this new laser (The maximum intensity was 250 kcps under the best condition with the Ar laser during the K^* experiment in 2007 [22].).

3.3 Lead-plastic sandwich detector

Figure 8 and 9 show the experimental setup around the target. The detector consists of 5 layers of the combination of a plastic scintillator and a lead sheet (gamma counter), and one

Figure 7: Photo of the target system.

layer of a plastic scintillator (charge counter) placed at the inner side of the gamma counter. The angular coverage is from –174° to 20° in the polar angle.

The lead-plastic detector will count the number of charged particles and γ rays. Neither a measurement of energies of γ rays, nor particle identification is needed in this experiment. The inner diameter of the charge counter is 100 mm, and the outer diameter of the neutral counter is 175 mm. The counters are segmented into 12 sectors in the azimuthal angle. The plastic scintillator is 5 mm thickness and 630 mm length. The lead sheets are 5 mm thickness, and the conversion rate for the 5 layers is 97%. Figure 10 shows the schematic front view of the lead-plastic sandwich detector. A wave length-shifter (WLS) fiber (Kurare Y11(200)-M) will be adopted for readout. The scintillators have grooves in the z-direction (beam direction) with 1.2 mm width, 1.3 mm depth and 5 mm (10 mm) spacing in the charged counters (gamma counters) for the WLS with the 1 mm diameter. About 10 photoelectrons with one fiber are expected for one minimum ionization particle [21]. We have four fibers for the charge counter, and 20 fibers for the gamma counters in one segment. The PM tubes will be attached to the upstream side of scintillators. One multi-anode PM tube with 16 channels will be used for 12 charge counters. The one channel of the multi-anode PMT has a space for 4 fibers (4 mm × 4 mm). The twelve PM tubes (1 inch or 2 inch) will be used for the gamma counters.

3.4 Identification of reaction modes

The lead-plastic sandwich detector will be installed around the target to detect charged particles and γ rays from mesons. Table 1 shows a list of the final states for proton photoproductions. The number of charged particles, and γ rays for each reaction are summarized in the table. According to the number of charged particles and γ rays, reactions are organized to three modes, A, B, and C. By obtaining the missing mass spectra in each mode, the specific reactions will be observed with less background events. The acceptances of the lead-plastic detector for each reaction are summarized in Table 2. The acceptances include the decay branching ratio of mesons. The acceptances depend on the energy and the scattering angle, and change by about

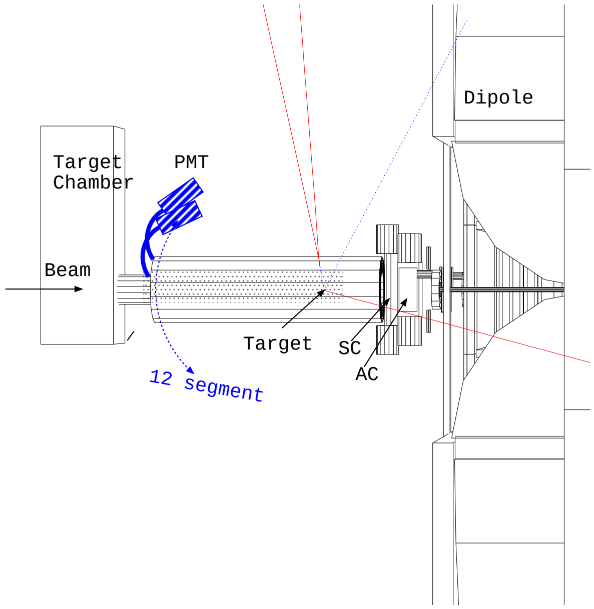

Figure 8: Side view of the experimental setup. start counter (SC) and aerogel counter (AC) are located between the lead-plastic sandwich detector and the forward spectrometer.

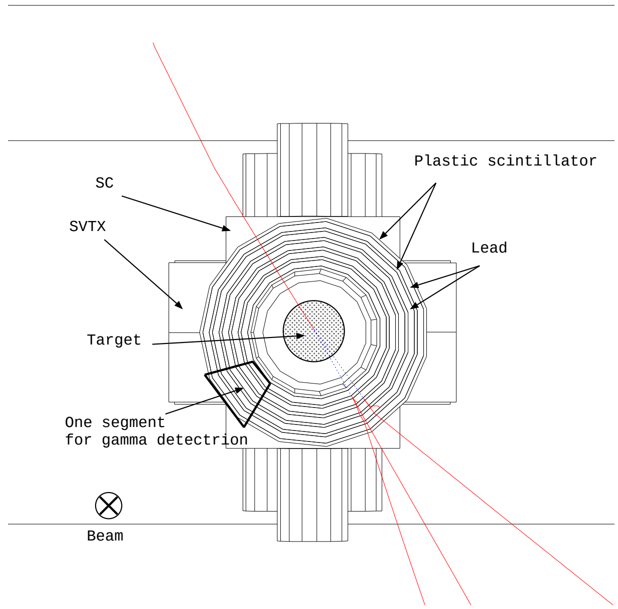

Figure 9: Front view of the experimental setup. SVTX means the silicon vertex detector.

5%. Figure 12 shows the expected missing mass square in each mode at E_γ = 2.3 – 2.4 GeV and cos$\Theta_{c.m.}$ = -0.9 – -1.0.

- A mode for a detection of π^0 and η mesons.
  A requirement is no charged particles, and less than 7 γ rays. Events from $2\pi^0$ and $4\pi^0$ productions remain as backgrounds. About 10% of ω, η' and ϕ mesons in the neutral mode remain.

- B mode for ρ^0 and ϕ mesons.
  A requirement is no γ rays, and the number of charged particles is from 1 to 3. Events from $\pi^+\pi^-$ (∼80%) and $\pi^+\pi^-\pi^+\pi^-$ (∼20%) productions remain as backgrounds. As a option for a detection of ϕ mesons, we will install an additional layer of plastic counters more inside of the detectors covering the angular range of $\theta_{lab} < 60°$ in the laboratory system. Most of Kaons from ϕ mesons are scattered in $\theta_{lab} < 60°$, while $\pi^+\pi^-$ events have more broad angular distribution as shown in Fig. 11. When charged particles at $\Theta_{lab} < 60°$ are selected, about a half of $\pi^+\pi^-$ events are rejected, and the ϕ peak will be more clearly observed. This is B' mode.

- C mode for ω and η' mesons. A requirement is more than one γ rays, and more than one charged particles. Background events are mainly from 3π and $\pi^+\pi^-\pi^0\pi^0$ productions. A part of η mesons in this mode remain.

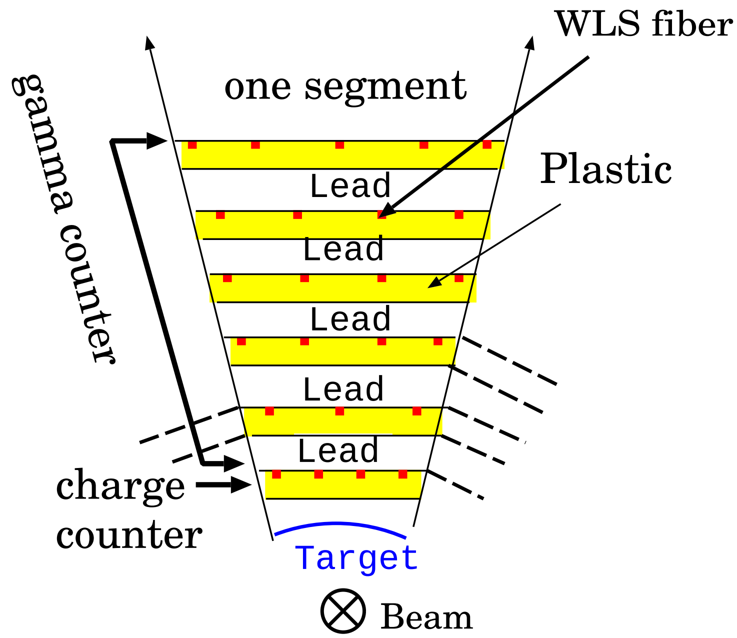

Figure 10: Front view of one segment of the lead-plastic sandwich detector with the WLS fiber setting.

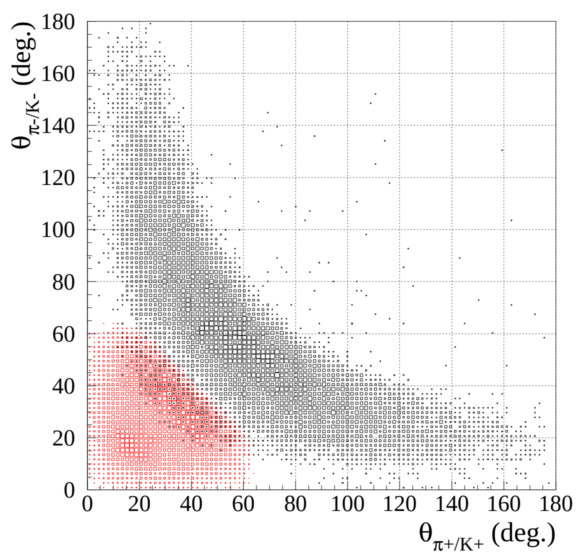

Figure 11: Scattering angles, θ_{lab}, for non-resonant 2π production (black) and K^+K^- (red) from ϕ mesons obtained with MC simulation.

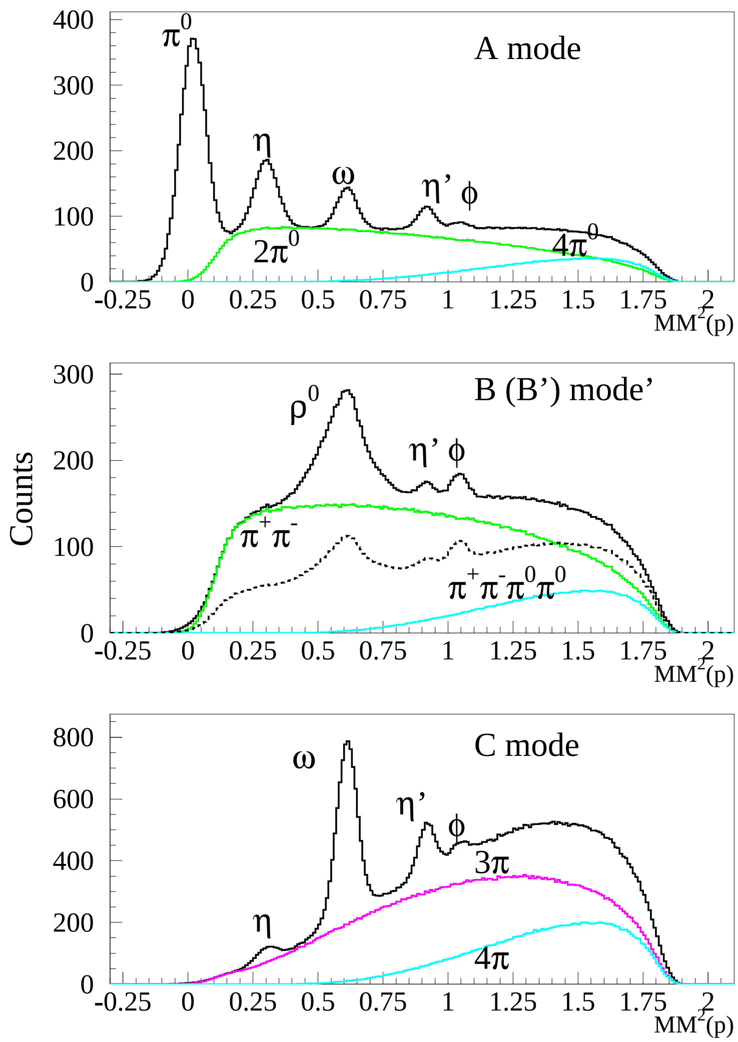

Figure 12: Expected missing mass spectra for each mode at $E_\gamma = 2.3 - 2.4$ GeV and $\cos\Theta_{c.m.} = -0.9 - -1.0$. The green, pink and light-blue curves are for backgrounds from 2π, 3π and 4π productions, respectively. The dashed curve is for B' mode.

Table 1: List of reaction modes. The first column shows mesons in the final states for the $\gamma p \to pX$ reaction.

Mesons	Branching(%)	charged	γ (Yes/No)	Mode	Other mode
$\pi^0 \to 2\gamma$	98	0	2 (Y)	A	–
$\eta \to 2\gamma, 3\pi^0$	72	0	2, 6 (Y)	A	C ($\pi^+\pi^-\pi^0$)
$\rho^0 \to \pi^+\pi^-$	100	2	0 (N)	B	–
$\omega \to \pi^+\pi^-\pi^0$	89	2	2 (Y)	C	A ($\pi^0\gamma$)
$\eta' \to \pi^+\pi^-\eta$	74	2	2 (Y)	C	A ($2\pi^0\eta$)
$\phi \to K^+K^-/K^0K^0$	49/34	2	0 (N)	B/C	
$\pi^0\pi^0$	33	0	4 (Y)	A	
$\pi^+\pi^-$	67	2	0 (N)	B	
$\pi^+\pi^-\pi^0$	100	2	2 (Y)	C	
$\pi^0\pi^0\pi^0\pi^0$	11	0	8 (Y)	A	
$\pi^+\pi^-\pi^+\pi^-$	44	4	0 (N)	B	
$\pi^+\pi^-\pi^0\pi^0$	44	2	4 (Y)	C	

Table 2: Acceptance (%) for each reaction mode.

Channel	A mode	B mode	B' mode	C mode
$\pi^0 \to 2\gamma$	.92	.02	.01	.06
$\eta \to 2\gamma, 3\pi^0$	.65	.03	.01	.30
$\rho^0 \to \pi^+\pi^-$	.00	.73	.27	.24
$\omega \to \pi^+\pi^-\pi^0$	.09	.06	.03	.80
$\eta' \to \pi^+\pi^-\eta$	.14	.07	.04	.65
$\phi \to K^+K^-$	.11	.31	.24	.45
$\pi^0\pi^0$	.93	.00	.00	.07
$\pi^+\pi^-$	.00	.76	.29	.21
$\pi^+\pi^-\pi^0$	.01	.09	.05	.85
$\pi^0\pi^0\pi^0\pi^0$	.74	.00	.00	.12
$\pi^+\pi^-\pi^+\pi^-$	.00	.25	.32	.14
$\pi^+\pi^-\pi^0\pi^0$	.02	.01	.01	.90

4 Request for beam

4.1 Estimation of the beam time requested

The cross section for ϕ photoproduction is expected to be the smallest in $\pi^0, \eta, \eta', \omega, \rho^0$, and ϕ channels. The cross section is estimated to be 0.01 μb/sr from the small ϕ peak seen in Figure 2. The yield is estimated as follows:

$$Yield = \frac{d\sigma}{d\Omega} \times A \times B \times N_p \times N_\gamma \times T \times 0.4 \times 2\pi \quad (1)$$

$$= 0.01 \times 10^{-30} \times 0.5 \times 0.31 \times 6.8 \times 10^{23} \times 5 \times 10^5 \times 0.4 \times 2\pi \sim 1 \times 10^{-3} \text{ events/s.} \quad (2)$$

A is the acceptance of the forward spectrometer for protons, and it is about 0.5 for the range of $0.6 < \cos\Theta^{p}_{c.m.} < 1.0$. B is the acceptance of the lead-plastic detector for $\phi \rightarrow K^{+}K^{-}$, 0.31 (see Table 2). N_p is the number of protons in the target, 6.768 $\times 10^{23}$. N_γ is the number of tagged photons, 500 kcps, and T is a transmission for the photon beam, 0.5. The solid angle for proton detection is 0.4 of $0.6 < \cos\Theta_{c.m.} < 1.0$. s This yield is for $E_\gamma = 1.5 - 2.9$ GeV and $-1 < \cos\Theta_{c.m.} < -0.6$. When we use a bin size of $d\cos\Theta_{c.m.} = 0.1$ and $dE_\gamma = 0.1$ GeV, we will have 1.13 $\times 10^{-5}$ event/s = 0.95 events/bin/day.

We will have about 85 ϕ events in each bin for 90 days beam time. This is enough to determine differential cross sections. We will use wider binning for a measurement of photon asymmetries. We will expect more yields for other channels, $\pi^0, \eta, \eta', \omega$, and ρ^0.

4.2 Experimental schedule

We require a three-day beam time for a preparation of side detectors and study of the trigger in addition to 90 days for physics run.

References

[1] S. Capstick, W. Roberts, Phys. Rev. D 49 (1994) 4570; S. Capstick, W. Roberts, Phys. Rev. D 58 (1998) 074011.

[2] K. Wijesooriya, *et al.*, Phys. Rev. C 66 (2002) 034614.

[3] O. Bartalini, *et al.*, Eur. Phys. J. A 26 (2005) 399.

[4] M. Dugger, *et al.*, Phys. Rev. Lett. 89 (2002) 222002.

[5] V. Crede, *et al.*, Phys. Rev. Lett. 94 (2005) 012004.

[6] R. Plotzke, *et al.*, Phys. Lett. B 444 (1998) 555.

[7] M. Dugger, *et al.*, Phys. Rev. Lett. 96 (2006) 062001.

[8] M. Sumihama, *et al.*, Phys. Lett. B 657 (2007) 32.

[9] R. Arndt, W. J. Briscoe, I. I. Strakovsky, and R. L. Workman, Phys. Rev. C 66 (1002) 055213; http://gwdac.phys.gwu.edu/.

[10] L. Tiator and S. Kamalov, nucl-th/0603012; D. Drechsel, O. Hanstein, S.S. Kamalov and L. Tiator, Nucl. Phys. A 645 (1999) 145; http://www.kph.uni-mainz.de/MAID/.

[11] T. Regge, Nuovo Cim. 14 (1959) 951.

[12] M. Guidal, M. Laget, M. Vanderhaeghen, Nucl. Phys. A 627 (1997) 645.

[13] M. Sumihama, technical note No. 39.

[14] R.W. Clifft, *et al.*, Phys. Lett. B 72 (1977) 144.

[15] A. I. Titov, *et al.*, Phys. Rev. C58 (1998) 2429.

[16] LEPS proposal, M. Fujiwara, *et al.*

[17] L.O. Abrahamian, *et al.*, Phys. Lett. B 48 (1974) 463.

[18] P.J. Bussey, *et al.*, Nucl. Phys. B 154 (1979) 492.

[19] P.J. Bussey, *et al.*, Nucl. Phys. B 104 (1976) 253.

[20] J. Alspector, *et al.*, Phys. Rev. Lett. 28 (1972) 1403.

[21] Y. Tajima, *et al.*, Nucl. Inst. Meth. A 592 (2008) 261.

[22] LEPS proposal for Q-PAC, Q022, K. Hicks and K. Joo.